Controls on upper ocean salinity variability in the eastern subpolar North Atlantic during 1992–2017

Ali H. Siddiqui[1], Thomas W. N. Haine[1], An T. Nguyen[2], Martha Buckley[3]

[1]Department of Earth and Planetary Sciences, Johns Hopkins University, Baltimore, MD, USA
[2]Oden Institute for Computational Engineering and Sciences, University of Texas at Austin, Austin, TX, USA
[3]Atmospheric, Oceanic and Earth Sciences, George Mason University, Fairfax, VA, USA

Key Points:

- Two fresh anomalies observed in the eastern subpolar North Atlantic upper ocean during 1992–2017 share similar spatial characteristics.
- Salt budget analysis shows the 2012–2016 fresh anomaly in the upper 200 m occurs due to transport of anomalous salinity by mean currents.
- In contrast, the fresh anomaly in the 1990s is due to anomalous circulation of the mean salinity field.

Corresponding author: Ali H. Siddiqui, `asiddi24@jhu.edu`

Abstract

The eastern subpolar North Atlantic upper ocean salinity undergoes decadal fluctuations. A large fresh anomaly event occurred during 2012–2016. Using the ECCO state estimate, we diagnose and compare mechanisms of this low salinity event with that of the 1990s fresh anomaly event. To avoid erroneous interpretations of physical mechanisms due to reference salinity values in the freshwater budget, we perform a salt mass content budget analysis of the eastern subpolar North Atlantic. It shows that the recent fresh anomaly occurs due to the circulation of anomalous salinity by mean currents entering the eastern subpolar basin from its western boundary via the North Atlantic Current. This is in contrast to the early 1990s, when the dominant mechanism governing the fresh anomaly was the transport of the mean salinity field by anomalous currents across the southern boundary of the subpolar North Atlantic.

Plain Language Summary

On decadal time scales, the eastern subpolar North Atlantic shifts between a salty and fresh upper ocean. These changes are significant and need to be investigated because of their impacts on global ocean circulation and regional ocean biogeochemistry. Between 2012 and 2016, there was a large event where this region became fresher than it had been in over a century. A previous similar event occurred in the early 1990s, but with a smaller magnitude. We use a numerical model of the ocean to figure out why these events occurred. Our study shows that there were two different mechanisms at play. The recent event occurred because a lot of fresh water came in from the west by the mean currents. The 1990s event occurred because ocean currents shifted and brought fresh water from the south.

1 Introduction

Large scale low salinity events occur in the eastern subpolar North Atlantic Ocean (ESNA) on decadal time scales. Based on observations, the subpolar North Atlantic has been undergoing such decadal salinity changes since at least the early 20th century (Sundby & Drinkwater, 2007; Dickson et al., 1988; Dooley et al., 1984; R. Zhang & Vallis, 2006; Dickson et al., 1988; Belkin et al., 1998; Belkin, 2004). During the 1992–2017 period, there were two fresh anomaly events in the ESNA reaching maximum freshwater accumulation in 1995 and 2016 respectively.

We highlight previous discussion in the literature on mechanisms that control the salinity in the ESNA. Changes in the strength and size of the subpolar gyre (SPG) and local atmospheric forcing in the ESNA are proposed mechanisms involving processes local to the subpolar gyre (Fox et al., 2022; Holliday et al., 2020). Remote mechanisms to modulate the salinity in the ESNA on such time scales include advection of salt anomalies from the Arctic or the subtropics (J. Zhang et al., 2021; Yeager et al., 2012; Häkkinen et al., 2011; Thierry et al., 2008; Sundby & Drinkwater, 2007; Holliday, 2003).

The strength and size of the subpolar gyre has been hypothesized to play an important role in setting the salinity variability in the ESNA (Holliday, 2003; Hátún et al., 2005; Häkkinen & Rhines, 2004; Sarafanov et al., 2008; Yeager et al., 2012; Häkkinen et al., 2011; Thierry et al., 2008), especially in the context of the warming and salinification that occurred in the mid 1990s to 2000s. The expansion of the SPG reduces the contribution of salty subtropical waters to the ESNA, reducing the salinity; in 1994 and 2016 sea surface height (SSH) contours show an expanded subpolar gyre and fresh anomalies in the ESNA (Fig. 1). In contrast, the contraction of the SPG allows more subtropical waters into the ESNA, increasing salinity; in 2008 the subpolar gyre is contracted, as SSH contours retreat westward, and the ESNA is saltier (Fig. 1).

Subsequent studies have refined diagnostics for studying the relationship between the subpolar gyre strength and ESNA salinity; rather than considering SSH-based indices of the subpolar gyre strength ((e.g., Häkkinen & Rhines, 2004)), Tesdal et al. (2018) analyze a density-based gyre index, which is a proxy for the baroclinic strength of the gyre (Koul et al., 2020). Foukal and Lozier (2017, 2018) suggest that the salinity in the ESNA is more strongly influenced by the intergyre transport, which is modulated by the Atlantic meridional overturning circulation (AMOC). Koul et al. (2020) perform Lagrangian tracking experiments based on multiple definitions of the SPG strength during 1993–2016 and conclude that 64.8% virtual floats reaching ESNA originate from subtropical waters. Contributions from subpolar-sourced waters increase five-fold during an expanded state of the SPG, however.

Another method to diagnose mechanisms controlling temperature and salinity variability is by performing budget calculations. To address the decadal SST variability in the subpolar North Atlantic, Piecuch et al. (2017) calculated the heat budget for 46°–65°N and concluded that the warming in the late 1990s and subsequent cooling since 2008 is primarily driven by oceanic advective flux convergence. The anomalous flux convergence is dominated by anomalies across the southern boundary (46°N). Similar studies by Oldenburg et al. (2018) and Tesdal and Haine (2020) reach the same conclusion on the dominance of the southern boundary advection in setting subpolar North Atlantic heat and freshwater variability. However, the role of the AMOC is unclear in this mechanism. Similarly, Sanders et al. (2022) investigate the 2015 anomalous cooling in the eastern and central subpolar region (defined over 50–20°W, 43–63°N) using a mixed layer heat budget. They observe that surface heat loss initiates and drives the cooling, with advection sustaining the anomaly in the region (as expected from Tesdal and Abernathey (2021)). They also emphasize the role of vertical diffusion across the base of the mixed layer in the re-emergence of the anomaly during summer of 2014.

Bryden et al. (2020) observed that there has been a mean increase of 0.12 ± 0.04 Sv of freshwater flux (relative to a reference salinity of 35.17 psu) after 2010 compared to before 2009. This increase is about 10% of the 2004–2009 average flux. They propose that a freshening of 0.062 ± 0.013 Sv over the eastern subpolar gyre during 2014–16 relative to 2007–09 is primarily due to the reduction of the AMOC by 2.5 Sv after 2009.

So far, we have discussed how circulation variability within the Atlantic basin contributes to salinity anomalies in the ESNA. For the 2012–2017 freshening event, Holliday et al. (2020) describe the primary mechanism of net freshwater gain in the upper 200 m of the Iceland basin as the rerouting of Arctic-sourced Labrador Current water into the northern branch of the North Atlantic Current (NAC; Reverdin et al., 2003). It is modulated by changes in the SPG strength driven by changes in atmospheric forcing. Recently, Fox et al. (2022) highlighted that reduced surface heat loss led to an increase in warmer (less dense) waters in the Labrador Sea. The transport of these less dense waters from the upper ocean layers through the Labrador Current along with reduced volume transport from the Gulf Stream drove the cooling and freshening in the eastern subpolar region.

However, some studies suggest an important role for interactions between the subpolar North Atlantic and the Arctic. J. Zhang et al. (2021) and Sundby and Drinkwater (2007) attribute ESNA freshening events during 1983–1995 and 1947–2000 to the export of freshwater buildup in the Arctic. They suggest that sea ice and liquid freshwater anomalies travel via the Fram Strait and Davis Strait to the Labrador Sea and circulate around the eastern subpolar gyre in the North Atlantic Current. The proposed mechanism of freshwater buildup in the 1990s is increased freshwater flux from the Davis Strait (Belkin, 2004), which entered the Labrador Sea and propagated around the eastern subpolar gyre (Sundby & Drinkwater, 2007).
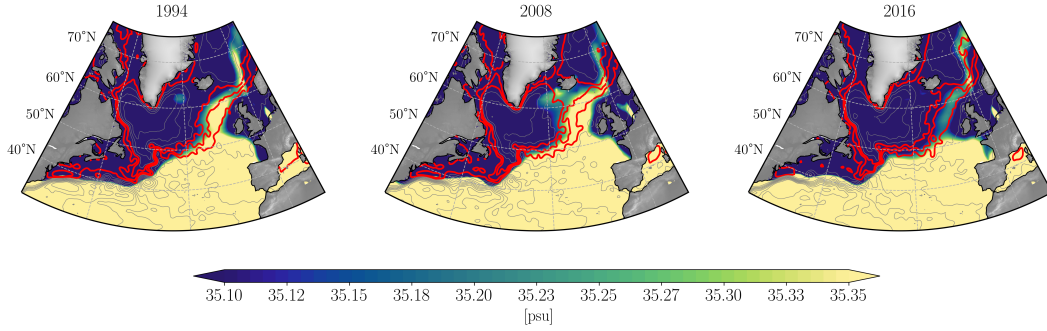
Figure 1: Annually-averaged subpolar North Atlantic upper-ocean salinity (0–200 m, colors) and sea-surface height (SSH; contours) averaged over one year preceding the salinity field. The SSH field is from the AVISO dataset and the salinity field is from the EN4 product. Following Chafik et al. (2019), the grey contours range from -0.8 m to 0.8 m with a spacing of 0.1 m and represent the mean dynamic topography (CNES-CLS2013 MDT). The red contours are -0.3, -0.2, -0.1 m and represent the three branches of the NAC. A Gaussian filter is used to smooth the SSH field with a scale of 1.25°. Modified from Fig. 3 of Weijer et al. (2022).

In this paper, we focus on what sets the upper ocean salinity in the ESNA on decadal time scales with emphasis on the two recent freshening events in the 1990s and 2010s using observations and modelling tools. We look at salt content anomaly budgets to explore oceanic mechanisms and further investigate the contribution of surface freshwater forcing in setting upper ocean salinity in the region.

In section 2 we discuss the methods used in this paper and investigate upper ocean salinity variability as seen in observations. In section 3, we compare and contrast the two fresh anomaly events observed during 1992–2017 using observations and ocean state estimates. We then diagnose the salinity variability using salt budget analysis for the ESNA and discuss potential mechanisms for the salinity variability.

2 Methods

2.1 Datasets

The main tool for our analysis of upper ocean salinity is the ECCO (Estimating the Circulation and Climate of the Ocean) version 4 release 4 (Forget et al., 2015) and ASTE (The Arctic Subpolar Gyre sTate Estimate) release 1 (Nguyen et al., 2021) ocean state estimates. The ECCOv4r4 state estimate (ECCO Consortium et al., n.d.) is a dynamically-consistent, data-constrained solution of the MITgcm model for the period 1992–2017. This allows for the construction of realistic closed budgets of volume, heat and salt. The horizontal resolution is 1°. ASTE_R1 is also a data-constrained ocean-sea ice model-data output that covers the Arctic Ocean and Atlantic ocean with lateral boundaries at 47.5°N in the North Pacific and 32.5°S in the South Atlantic for 2002–2017; the ASTE_R1 horizontal resolution is 1/3°.

We utilize a number of observational datasets to evaluate ECCOv4r4 and ASTE_R1. First, we compare to the EN4 hydrographic dataset (Good et al., 2013), which is an observational product compiled by the UK Met office. We use data from two hydrographic surveys to evaluate the performance of ECCOv4r4 for our analysis. The Extended EL-LET line (Holliday & Cunningham, 2013) is a section from Iceland to Scotland and the OVIDE line (Daniault et al., 2016) is a combination of sections from the southern tip

of Greenland to Portugal. These are the same sections used by Holliday et al. (2020).
We compare the salinity anomalies in the sections observed in the model data with the
ELLET and OVIDE sections. The data from the hydrographic survey carried out over
June–July, 2016 and May–June, 2016 for the OVIDE and ELLET line, respectively, is
compared with monthly-mean salinity anomaly from the model data. We consider the
upper 200 m annually-averaged ESNA salinity anomaly for 1992–2017 using the EN4 hy-
drographic dataset (Good et al., 2013) along with ECCOv4r4 and ASTE_R1 datasets.
The upper ocean 200 m is used to remain consistent with previous work that investigates
upper ocean salinity in the ESNA (Holliday et al., 2020; Koul et al., 2020).

We use ECCOv4r4 to track the evolution of salinity anomalies for the two fresh anomaly
events on monthly and also annual time scales. To investigate the mechanisms govern-
ing this evolution, we carry out salt budget analysis with ECCOv4r4 for the period 1992–
2017 for the entire subpolar North Atlantic (SPNA) and the ESNA. The salt budget anal-
ysis builds on the work by Buckley et al. (2014, 2015); Piecuch et al. (2017); Oldenburg
et al. (2018); Tesdal and Haine (2020); Nguyen et al. (2021) to investigate heat and salin-
ity variability in the subpolar North Atlantic.

The ESNA is defined as a box over 10–30°W, 46–65°N and the SPNA is defined
as the North Atlantic between 45°–65° N. Fig. 2 shows the location of the ESNA.

3 Results

In this section, we evaluate the ECCOv4r4 model data. Next, we consider the spa-
tial and temporal structure of the fresh anomaly events in the subpolar region. Then we
investigate the salt budget results.

3.1 Evaluation of ECCOv4r4

Here we present a comparison of ECCOv4r4 to ship-based hydrographic sections.
Fig. 2a shows the positions of the OVIDE and ELLET sections overlaid with sea level
height anomaly contours from ECCO. In summer of 2016, the upper 1000 m of the Rock-
all Trough has the highest salinity in the ELLET section. The salinity decreases below
1000m, which is seen in both the observations and ECCO data (Fig. 3). ECCO overes-
timates the salinity in the upper 1000 m, however. This is also true on the OVIDE sec-
tion from the Reykjanes Ridge to the Iberian abyssal plain during summer of 2016. The
ECCO salinity in the Irminger Sea during summer of 2016 is realistic, however. ECCO
also captures the sub-surface salinity minimum over the Iberian abyssal plain. On the
ELLET section, ECCO overestimates the salinity in the 0–200 m Iceland Basin by around
0.06 psu, and underestimates it by 0.04 psu in the Rockall Trough. Similarly, on the OVIDE
section, ECCO overestimates the 0–200 m salinity in the ESNA control volume (Fig. 2)
by around 0.05 psu. The time series (Fig. 2) of 0–200 m depth-averaged salinity anoma-
lies for the ESNA in ECCO accurately shows the fresh anomaly observed during 2012–
2017 and 1992–1995 compared to EN4. The salinity difference between ECCO and EN4
is 0.027 ± 0.046 psu (from Fig. 2b, but using the absolute salinity values, not the anoma-
lies). The biases in the ELLET and OVIDE sections quoted above are consistent with
this ECCO/EN4 difference, and are relatively small compared to the salinity fluctuations
over time seen in Fig. 2b. This builds confidence in the use of ECCO for our analysis.
The only noticeable disagreement between EN4 and ECCO seen in Fig. 2b is during 1995–
1996, when the ESNA shows anomalous positive salinity anomalies in EN4, whereas ECCO
shows negative salinity anomalies. Spatial maps of 0–200 m salinity anomalies show a
large positive anomaly situated south of the Grand Banks in 1995 in both datasets (see
Supplemental Figs. 1–3). In EN4 this anomaly spreads throughout the ENSA in 1996,
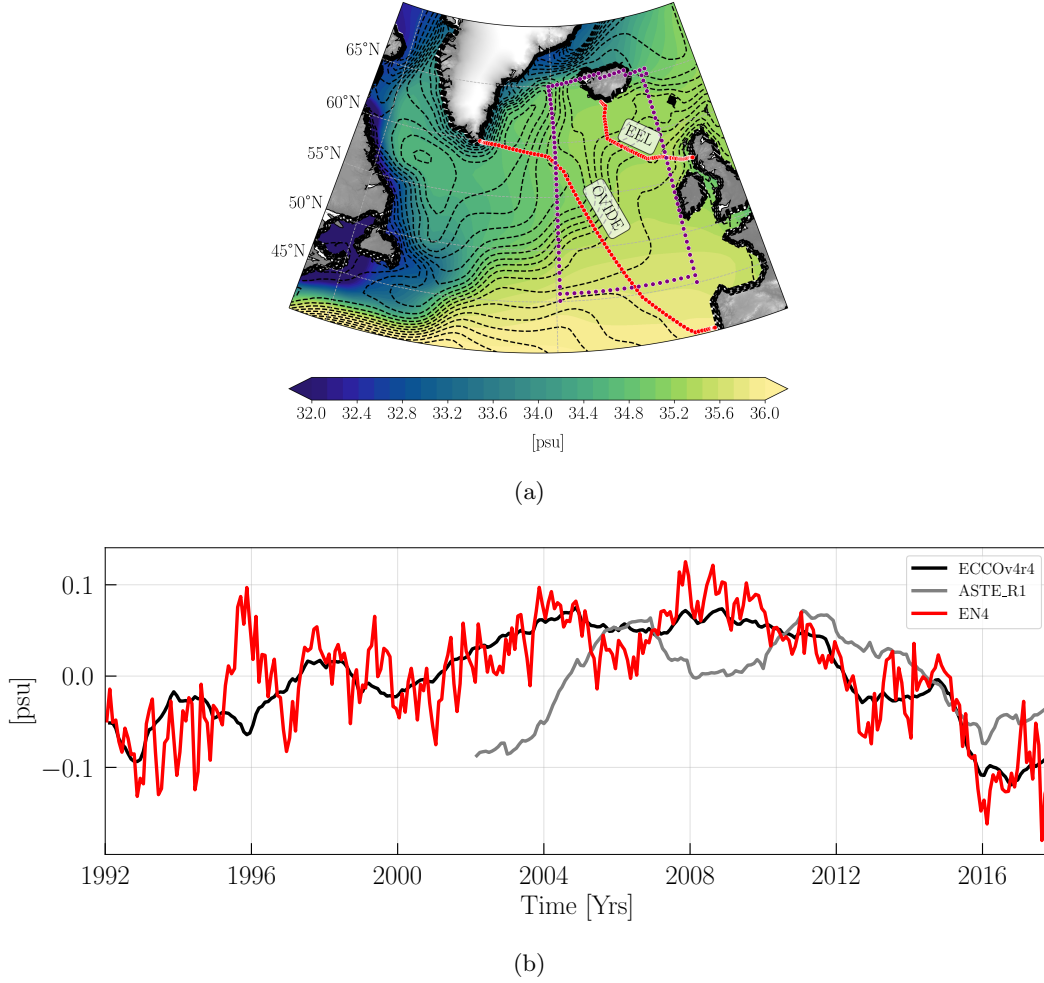but it does not spread so far east in ECCO.

(a)

(b)

Figure 2: (a) Subpolar North Atlantic (SPNA) sea level height anomaly contours (spacing of 0.04 m) in the ECCOv4r4 dataset averaged over 1992–2017. The Extended ELLET line (EEL) and OVIDE sections are also shown. (b) Upper ocean 200 m salinity anomaly time series for the eastern Subpolar North Atlantic (ESNA) from EN4 (red), ECCOv4r4 (black) and ASTE_R1 (grey) datasets. The ESNA is defined as 45–65°N, 10–30°W (purple box in (a)).

3.2 Spatial and Temporal Structure of Upper Ocean (S_{200}) Salinity Anomalies

We first establish the occurrence of two fresh anomalies in the upper 200 m of the ESNA using the ECCOv4r4, ASTE_R1, and EN4 datasets (Fig. 2). We observe a fresh anomaly in the ESNA in the early 1990s, after which there is a prolonged period of salinification until 2011, and a reversal to freshening thereafter. The first fresh anomaly event (F_1) is observed from 1992 until 1995 in EN4 and 1997 in ECCOv4r4. For the second fresh anomaly event (F_2), all three datasets show the Iceland basin salinity anomaly dropping below zero after 2012 until 2017. This is also reflected in the decadal cycle in the upper ocean salinity maps for the ESNA region in the ECCO, ASTE_1 and EN4 datasets

200 (see Supplemental Fig. 1–3). We label the 1990s fresh event as F_1 and the 2010s fresh
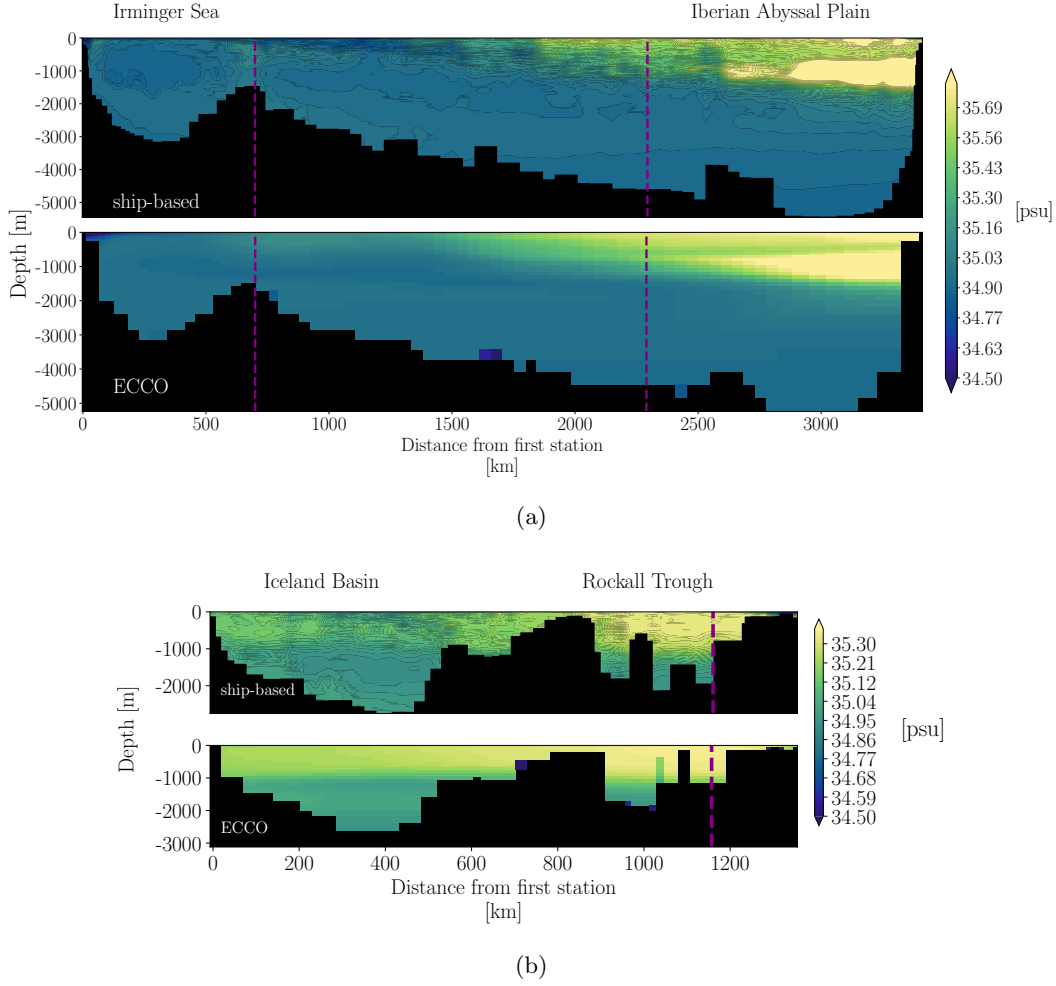201 event as F_2.

(a)

(b)

Figure 3: Comparison of ECCOv4r4 salinity for (a) June–July 2016 with the OVIDE section and (b) May–June 2016 with the ELLET line. The ECCOv4r4 salinity sections are taken at the same times as the field observations. Vertical purple lines indicate parts of the sections inside the ESNA control volume defined in Fig. 2 (for the OVIDE section 700–2290 km, and for the ELLET section 0–1150 km, are within the ESNA control volume). Colorbar limits are different for the two section plots.

202 Spatial trends in the upper ocean (S_{200}) salinity are computed using EN4 and EC-
203 COv4r4. During 2005–16, both products show a statistically significant freshening in the
204 ESNA at 95% confidence intervals using the student's t-distribution. ECCOv4r4 and EN4
205 disagree on trends in the Labrador Sea and the Grand Banks region, however (Fig. 4).

206 Next, we consider the annually averaged anomalies in the ECCO data and com-
207 pare the two fresh anomaly events, F_1 and F_2, which are shown in Fig. 5. As we trace
208 the freshwater event in the 1990s (F_1) we observe a fresh ESNA and saltier western sub-
209 polar gyre (SPG) in 1992. During 1993 and 1994, a fresh anomaly is situated in the Labrador
210 Sea, and in the Iceland Basin in 1995. By 1996, the signal fades away from the ESNA.
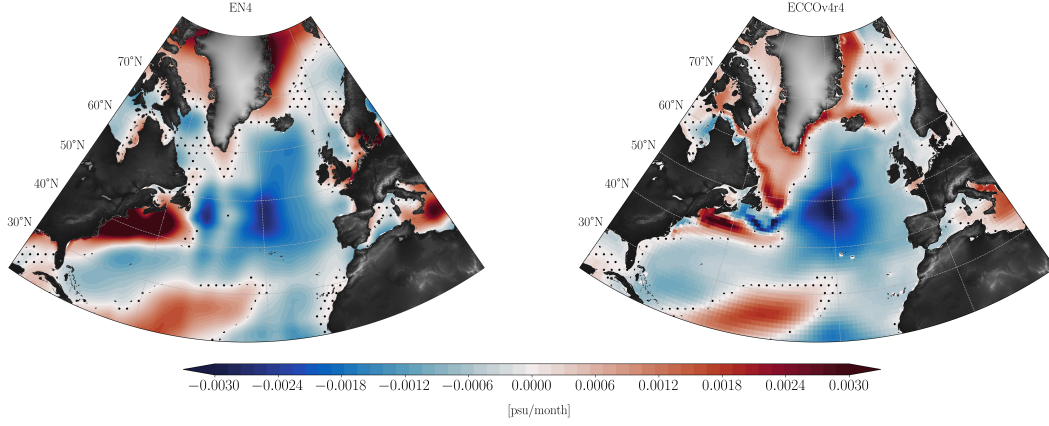
Figure 4: Spatial distribution of linear trends in the upper-ocean salinity (0–200 m) over 2005–2016 using monthly mean fields of (a) EN4 and (b) ECCOv4r4. Dotted regions display insignificant trends calculated using the students-t test with a p-value of 0.05.

The 2010s event, has a similar fresh anomaly in the Labrador Sea in 2013, and also in the Iceland Basin in 2016. Note that in both events, there is a positive salinity anomaly south of the Grand Banks region, preceding the maximum freshening in 1995 and 2016.
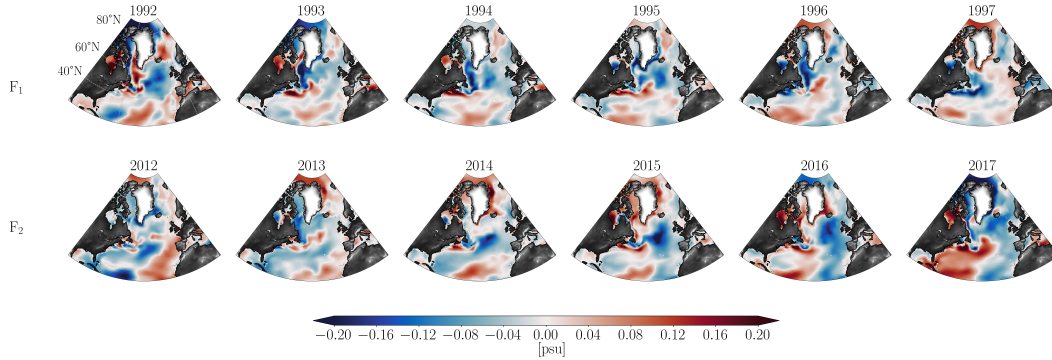

Figure 5: Annually averaged anomaly maps for the upper 200 m salinity (S_{200}) during 1992–1994 and 2012–2014 in ECCOv4r4.

We investigate this further using the ECCO data by tracking salinity anomalies along the western SPG and along the Gulf Stream with the Iceland Basin as a common terminus. We create a section following mean sea level anomaly contours around the subpolar gyre which begins south of Denmark strait. The section follows the -0.6 m mean sea level anomaly contour along the East Greenland Current around the southeast coast of Greenland. The section continues along the West Greenland Current to the entrance of Baffin Bay, where it retroflects and follows the Baffin Island Current, eventually reaching the Labrador Sea. At this point, the section follows the -0.8 m mean sea level anomaly contour as it retroflects east of the Flemish Cap and follows the path of the northern branch of the NAC to the Iceland basin. This section represents a potential subpolar pathway for the anomaly propagation.

To investigate the salinity anomalies along a potential subtropical pathway, we create a section along the Gulf Stream which also terminates in the Iceland Basin. Both sections are inspired by the Lagrangian studies carried out by Burkholder and Lozier (2014); Foukal and Lozier (2018); Koul et al. (2020); J. Zhang et al. (2021) where passive tracers are tracked to the Iceland basin in a variety of experiments.
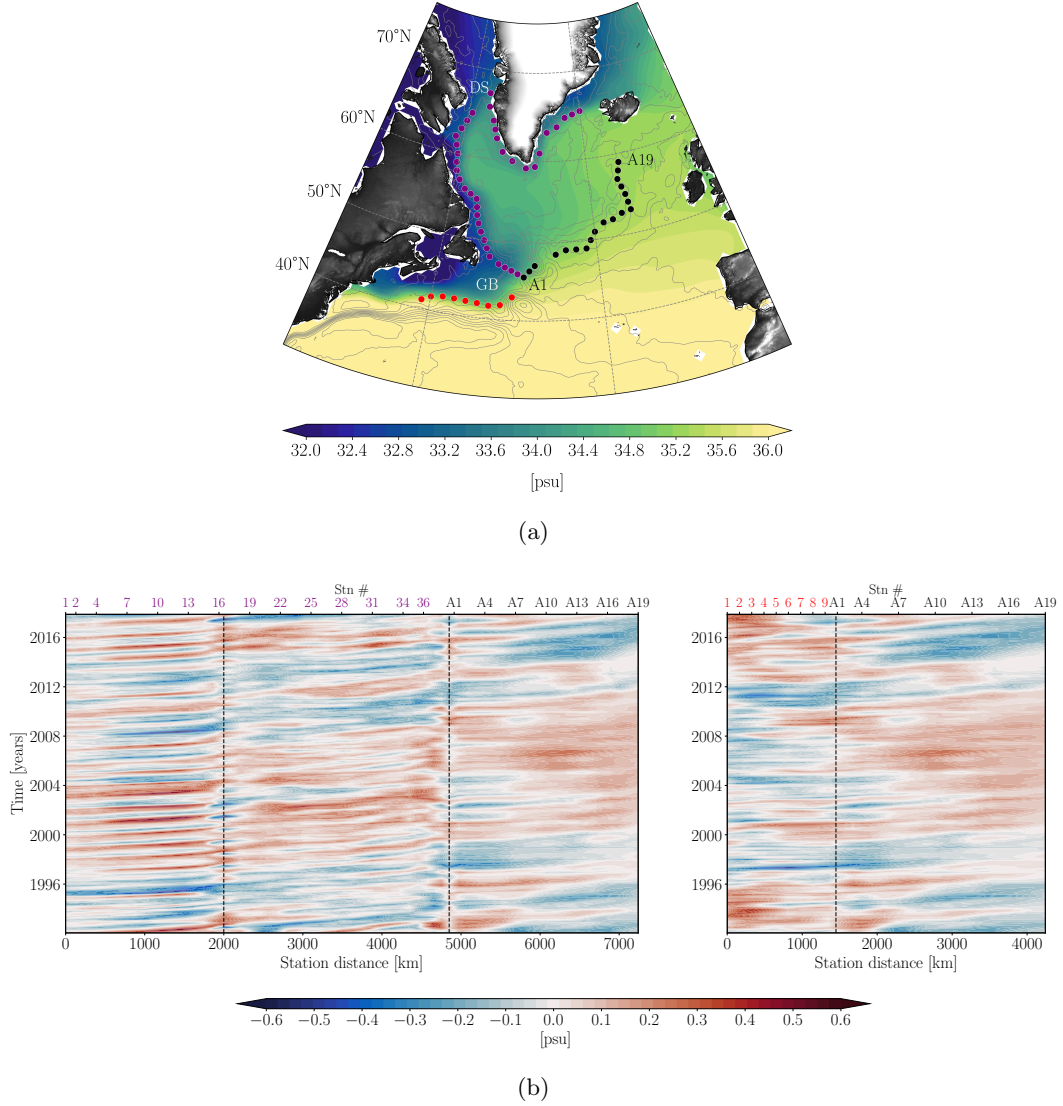

(a)

(b)

Figure 6: (a) Continuous sections along the western subpolar gyre boundary (purple; 56 stations) and along the Gulf Stream (red; 28 stations). The sections intersect at the NAC (station A1) and are merged from there to the Iceland Basin. (b) Hovmöller diagram of monthly salinity anomalies in the ECCO data along the sections. Vertical dashed lines are shown at Davis Strait (DS) and the Grand Banks (GB) region.

We first inspect the subtropical section. We find that there is a general tendency for there to be salinity anomalies of opposite sign along the Gulf Stream path and in the subpolar gyre, as noted by prior studies (Buckley et al., 2014; Joyce & Zhang, 2010; Sanchez-

Franks & Zhang, 2015; Yeager, 2015; Hátún et al., 2009; R. Zhang, 2008; Nye et al., 2011; Yan et al., 2017, 2018). For both subpolar freshening events, there are positive salinity anomalies along the Gulf Stream path. This positive salinity anomaly signal south of the Grand Banks is also observed in the years preceding the fresh anomaly event in the annually averaged salinity anomaly maps (Fig. 5). Along the subpolar section, high frequency freshening/salinification events can be tracked from Denmark Strait along the East Greenland Current and West Greenland Current. These represent seasonal fluctuations along the Greenland coast. Along the Labrador Current (from Davis Strait to the Grand Banks), the characteristics of the freshening/salinification events changes with lower-frequency variations than seen along the East and West Greenland Currents. From the Grand Banks to the Iceland Basin, the freshening/salinification events are at even lower frequencies. The relationship between salinity anomalies in the Icelandic Basin and those in the East/West Greenland Current and Labrador Current is complex, with some indications of signal propagation along the subpolar gye pathways, as suggested by Holliday et al. (2020) and Fox et al. (2022). We can now explore the role of circulation changes quantitatively by constructing a salt mass budget for the region.

3.3 Salt Budget Analysis

We construct a budget of the salt mass, an extensive quantity, which has a more accurate closure in the ECCO model output than a budget of salinity, an intensive quantity. The role of surface freshwater in the form of P-E+R (Precipitation-Evaporation+Runoff) is analyzed separately in a salinity budget calculation. We also avoid analyzing freshwater budgets due to ambiguities associated with reference salinity in such calculations (Schauer & Losch, 2019).

The salt conservation equation for the non-linear free surface in ECCOv4r4 is expressed in $z^\star$ coordinates (see equation (3) in Forget et al. (2015)). In $z^\star$ coordinates, sea surface height variations, η, are proportionally divided between ocean layers: $z^\star = (z - \eta)/(H + \eta)$ (equation (1) in Piecuch (2017)), where z is the fixed vertical coordinate and H is the ocean depth.

We express the volume and time integrated salt content, $M(t)$, for the control-volume V as

$$M(t) \equiv \underbrace{\rho_0 \int_{t^\star=0}^{t^\star=t} \int_V \frac{\partial (s^\star S)}{\partial t} \, dV^\star \, dt^\star}_{\text{Salt Mass}} = \underbrace{\rho_0 \int_{t^\star=0}^{t^\star=t} \int_V -\nabla_{z^\star} \cdot (s^\star S \mathbf{v}_{res}) - \frac{\partial (S w_{res})}{\partial z^\star} \, dV^\star \, dt^\star}_{\text{Advection}}$$

$$+ \underbrace{\rho_0 \int_{t^\star=0}^{t^\star=t} \int_V s^\star \mathcal{F}_S \, dV^\star \, dt^\star}_{\text{Forcing}} + \underbrace{\rho_0 \int_{t^\star=0}^{t^\star=t} \int_V s^\star (D_{\sigma,S} + D_{\perp,S}) \, dV^\star \, dt^\star}_{\text{Diffusion}}. \quad (1)$$

In this equation $s^\star = 1 + \eta/H$ is a scaling factor, $\nabla_{z^\star}$ indicates the gradient at constant $z^\star$, $(\mathbf{v}_{res}, w_{res})$ are the residual velocity fields defined as the sum of the Eulerian and bolus velocities, $\mathcal{F}_S$ is the forcing at the surface due to surface salt exchange due to sea ice melting/formation and a redistribution of the surface flux in the vertical column, and $D_{\sigma,S}$ and $D_{\perp,S}$ are diffusive processes parameterized along iso-neutral and vertical directions, respectively. We consider V to be the upper 200 m in the ESNA; we also consider the upper 200 m for the whole SPNA (this assumption is tested below in section 3.4; see Appendix A for more details). Eq. (1) expresses that the total time integrated salt mass is balanced by the time integrated horizontal and vertical advective convergence of salt flux, diapycnal and isopycnal diffusion, and surface forcing. The four named terms are each computed individually from the ECCO output, which allows us to test the closure of (1). The ratio of the residual (left hand side minus right hand side) to the salt mass (left hand side) is of O(10^{-4}). Details on how to close the salt budget in the ECCO dataset are provided in Piecuch (2017).

We remove the mean seasonal cycle and a linear trend from all terms in the time integrated salt budget. This gives us the salt content anomaly time series, which is shown in Fig. 7 (labelled "salt anomaly"). We observe a negative salt content anomaly of the SPNA during 1992–1997 and 2012–2017. For the ESNA, the salt content anomaly remains negative during 1992–1997 and 2012–2017. The salt mass anomaly increases and reaches a maximum in 2004 for the entire SPNA, and in 2008 for the ESNA. We find that both the diffusion and advection terms contribute to the salt content anomaly, and these terms are strongly anti-correlated. The surface salt forcing (due to brine rejection) has a negligible impact.

From 1995–2000 and 2004–2012, the change in the diffusion term is larger than the change in the advection term in the SPNA, and it drives the salt mass change. For the ESNA, this is seen during 1995–2000 and 2008–2011. We highlight the years in yellow/blue when the advection term increases/decreases rapidly in the two basins.
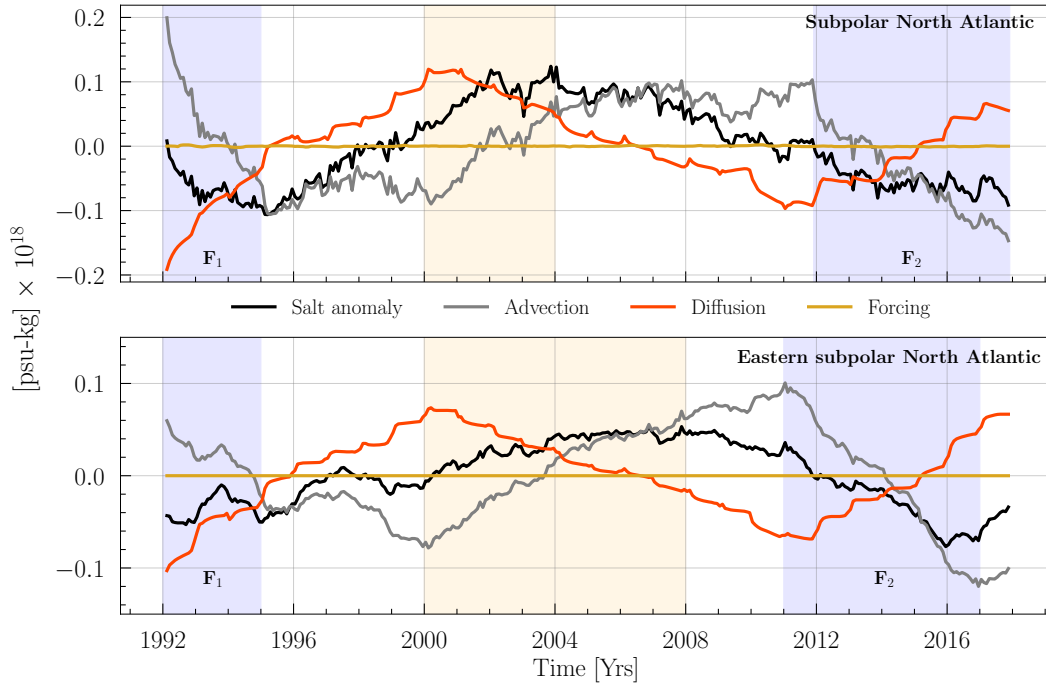

Figure 7: (a) Time and volume integrated salt anomaly budget for the upper 200 m of the (a) Subpolar North Atlantic and (b) the eastern subpolar North Atlantic (ESNA, see Fig. 2 for the definition of the ESNA). F_1 and F_2 are fresh anomaly events in the two basins during 1992–1997 and 2012–2017 respectively. Yellow/blue shading indicates periods of increased/decreased advection of salt mass.

We further investigate the advection and diffusion terms separately. We decompose the advection term into time-average and anomaly terms, following Dong and Sutton (2002); Doney et al. (2007); Buckley et al. (2015); Piecuch et al. (2017) and Tesdal and Haine (2020). We write the advection term $\mathcal{A}$ in (1), as $\mathcal{A} = \overline{\mathcal{A}} + \mathcal{A}'$, where the overbar denotes time averaging, i.e $\overline{\mathbf{v}} = \frac{1}{(t_f - t_i)} \int_{t_i}^{t_f} \mathbf{v} dt$ and the prime denotes departure from the time average. Initial and final time values in the averaging period are denoted by t_i and t_f. The averaging period is 1992–2017.

301   This decomposes the advection term into variability produced by changes in the
302 circulation ($\mathbf{v}'_{res}\bar{S}$), variability produced by changes in salinity ($\bar{\mathbf{v}}_{res}S'$), and that due
303 to the co-variability of the circulation with the salinity ($\mathbf{v}'_{res}S' - \overline{\mathbf{v}'_{res}S'}$).

304   We now express $\mathbf{v}_{res} = \mathbf{v}_e + \mathbf{v}_b$, i.e., the total velocity is the sum of Eulerian ($\mathbf{v}_e$)
305 and bolus ($\mathbf{v}_b$) velocities, and similarly for the vertical speeds (w_e, w_b). Re-arranging the
306 terms in Eq. (A2) gives:

$$
\mathcal{A}' = -\rho_0 \int^t \int_V \left\{ \underbrace{\left(\nabla_{z^\star} \cdot s^\star \bar{\mathbf{v}}_e S' + \frac{\partial(\bar{w}_e S')}{\partial z^\star} \right)}_{\bar{v}_e S'} + \underbrace{\left(\nabla_{z^\star} \cdot s^\star \mathbf{v}'_e \bar{S} + \frac{\partial(w'_e \bar{S})}{\partial z^\star} \right)}_{v'_e \bar{S}} + \right.
$$

$$
\underbrace{\left(\nabla_{z^\star} \cdot s^\star (\mathbf{v}'_e S' - \overline{\mathbf{v}'_e S'}) + \frac{\partial(w'_e S' - \overline{w'_e S'})}{\partial z^\star} \right)}_{v'_e S' - \overline{v'_e S'}}
$$

$$
\underbrace{\left(\nabla_{z^\star} \cdot s^\star \bar{\mathbf{v}}_b S' + \frac{\partial(\bar{w}_b S')}{\partial z^\star} \right)}_{\bar{v}_b S'} + \underbrace{\left(\nabla_{z^\star} \cdot s^\star \mathbf{v}'_b \bar{S} + \frac{\partial(w'_b \bar{S})}{\partial z^\star} \right)}_{v'_b \bar{S}} +
$$

$$
\left. \underbrace{\left(\nabla_{z^\star} \cdot s^\star (\mathbf{v}'_b S' - \overline{\mathbf{v}'_b S'}) + \frac{\partial(w'_b S' - \overline{w'_b S'})}{\partial z^\star} \right)}_{v'_b S' - \overline{v'_b S'}} \right\} dV^\star \, dt^\star + \epsilon. \quad (2)
$$

313   The sum of all the terms on the right hand side of Eq. (2) should equal the anomaly in
314 the convergence of advective salt flux, which is an output in ECCOv4r4. When we com-
315 pute the individual terms from monthly mean velocities and salinity (interpolated to the
316 model velocity grid points), however, it introduces a numerical error, which we call ϵ.
317 Volume integrated ratios of ϵ to each individual term are O(10^{-1}) (see Fig. 9) .

318   The advection anomaly term is shown in Fig. 8. For the whole SPNA, during the
319 F_1 event, the variability in the advective convergence term is dominated by the anoma-
320 lous Eulerian advection of mean salinity ($v'_e \bar{S}$). During 1992–1995, it is twice that of the
321 mean circulation of anomalous salinity ($\bar{v}_e S'$). For the F_2 event the mean bolus advec-
322 tion of anomalous salinity ($\bar{v}_b S'$) tends to drive the freshening, as the Eulerian terms bal-
323 ance each other out. Note that the advective convergences of anomalous circulation of
324 mean salinity and the mean circulation of anomalous salinity are anti-correlated during
325 both events. Anti-correlation of advective convergences due to salinity variations and due
326 to geostrophic velocity variations is expected when isobars and isohalines are aligned,
327 as shown for heat transport convergences by Buckley et al. (2015).

328   The decomposition of the anomalous advection term for the ESNA is different. The
329 F_1 negative salt anomaly is still dominated by the anomalous circulation of mean salin-
330 ity ($v'_e \bar{S}$). In contrast, the driver for the F_2 anomaly is the mean circulation of anoma-
331 lous salinity ($\bar{v}_e S'$). Also, unlike the SPNA, the anomalous circulation of mean salinity
332 is not anti-correlated to the mean circulation of anomalous salinity. This indicates that
333 either (1) the isobars and isotherms are not strongly aligned, which would occur if the
334 density field in the ESNA is only weakly dependent on salinity, or (2) there is a strong
335 contribution of agoestrophic transports to the advective convergences. For example, there
336 is no expected anticorrelation between salt transport convergences due to salinity vari-
337 ations and those due to Ekman velocity variations.

338   To further investigate the $\bar{v}_e S'$ term, we look at the decomposed anomalous advec-
339 tion for the ESNA in terms of flux entering the control volume from the boundaries. We
340 rewrite Eq. (A2), apply the Gauss-divergence theorem, and express the divergence of anoma-
341 lous advection in the ESNA as a sum of salt fluxes across the four lateral boundaries and
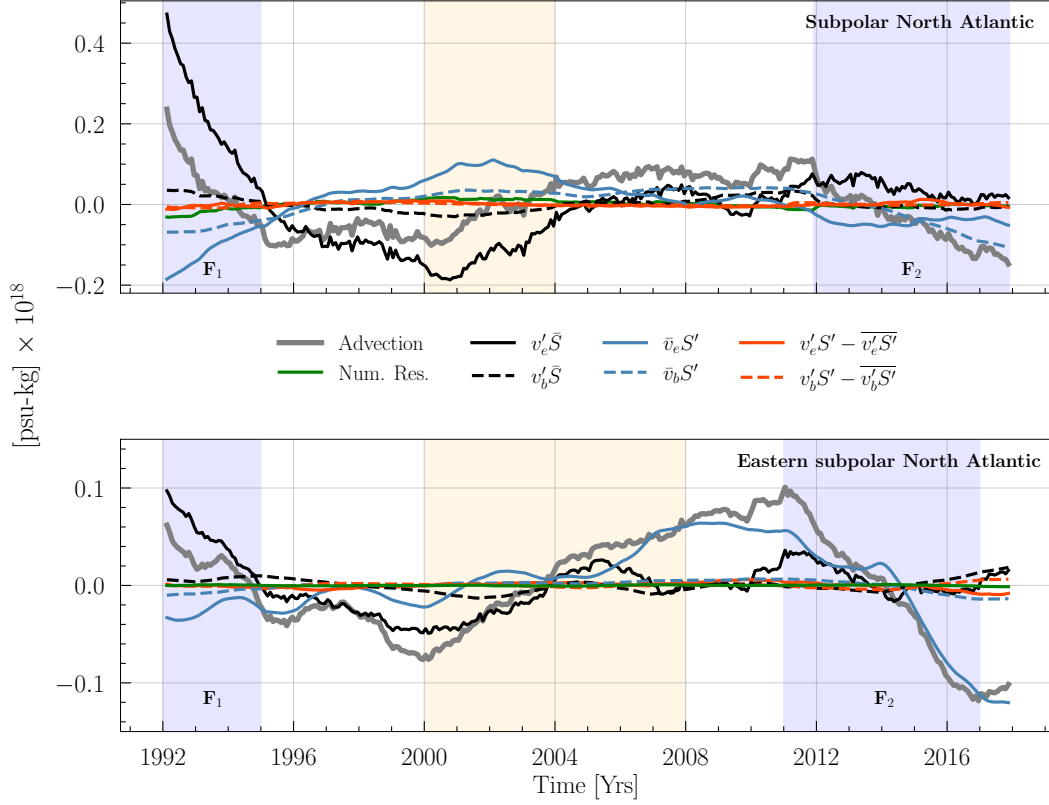
Figure 8: Decomposition of the anomalous advection term $\mathcal{A}'$ in the salt budget for the upper 200 m of the (a) Subpolar North Atlantic and (b) Eastern subpolar North Atlantic (ESNA, see Fig. 2 for the definition of the ESNA). The anomalous advection term is decomposed into contributions from: changes in the circulation ($v'_{res}\bar{S}$), changes in the salinity ($\bar{v}_{res}S'$), and changes due to the co-variability of the circulation with the salinity ($v'_{res}S' - \overline{v'_{res}S'}$). This decomposition is made for both Eulerian and bolus velocity components. See Eq. (2) for details on the terms, and see also Fig. 7 for information on the full salt budget. F_1 and F_2 are fresh anomaly events in the two basins during 1992–1997 and 2012–2017 respectively. Yellow/blue shading indicates periods of increased/decreased advection of salt mass.

across the 200 m vertical boundary:

$$\mathcal{A}' = -\rho_0 \int^t \int_B [\underbrace{s^\star \bar{\mathbf{v}}_{res}S' + \bar{w}_{res}S'}_{\bar{v}S'} + \underbrace{s^\star \mathbf{v}'_{res}\bar{S} + w'_{res}\bar{S}}_{v'\bar{S}} +$$

$$\underbrace{s^\star(\mathbf{v}'_{res}S' - \overline{\mathbf{v}'_{res}S'}) + (w'_{res}S' - \overline{w'_{res}S'})}_{v'S' - \overline{v'S'}} \cdot \hat{\mathbf{n}}] \, dB \, dt^\star. \quad (3)$$

Here, B represents the four lateral surfaces, i.e., south, north, east and west, along with the vertical boundary at 200 m. The $\bar{v}_e S'$ term across each face is also decomposed into contributions from Eulerian and bolus components. These components are shown in Fig. 9. We observe that during F_2, there is an anomalous Eulerian salt flux ($\bar{v}S'$) entering the western boundary. It is responsible for bringing saltier water as $\bar{v}S'$ along the NAC. This is in contrast to the F_1 event where the advection is driven by the $v'\bar{S}$ term. A balance between the Eulerian flux of $v'\bar{S}$ across the southern and western boundaries along with
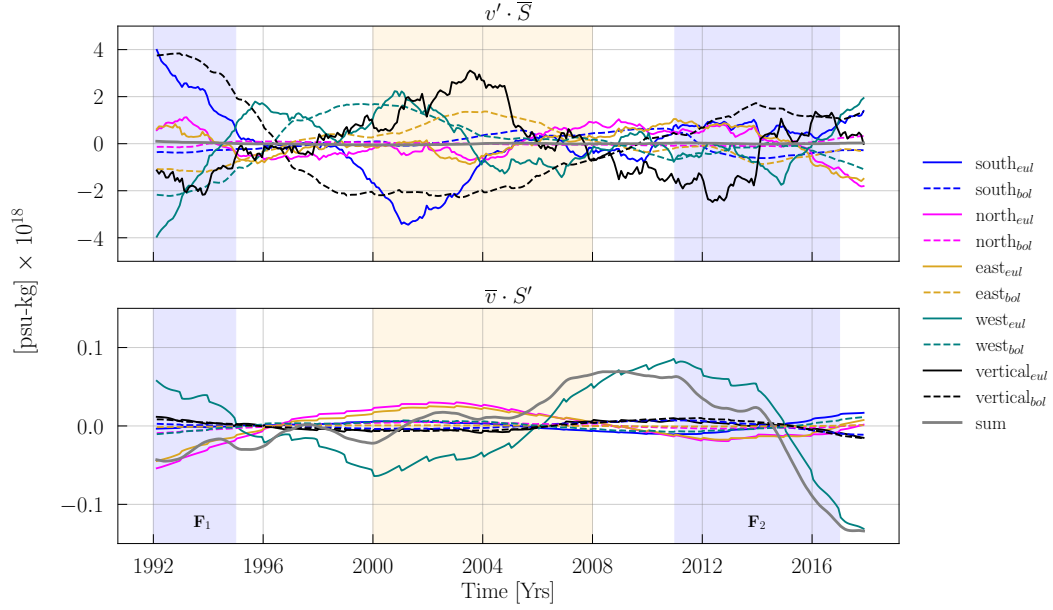
Figure 9: Decomposition of the anomalous advection term $\mathcal{A}'$ in the salt budget for the upper 200 m of the ESNA across the lateral and vertical boundaries. Shown here is the contribution from changes in the circulation with a mean salinity field ($v'\overline{S}$) and changes in salinity along mean flow ($\bar{v}S'$). This decomposition is made for both Eulerian and bolus velocity components. See Eq. (3) for details on the terms, and see also Fig. 7 for information on the full salt budget. F_1 and F_2 are fresh anomaly events in the two basins during 1992–1997 and 2012–2017 respectively. Yellow/blue shading indicates periods of increased/decreased advection of salt mass.

354 the bolus flux across the 200 m horizon keep the ESNA fresh. This is the major differ-
355 ence between the two events.

356   The diffusion component of the salt mass anomaly budget is expressed as

$$357 \qquad \mathcal{D}' = \rho_0 \int^t \int_V s^\star \underbrace{(D_{\sigma,S}}_{\mathrm{D}_H} + \underbrace{D_{\perp,S})}_{\mathrm{D}_V} \, dV^\star dt^\star. \tag{4}$$

358 Fig. 10 shows the decomposition of the diffusion term into vertical and horizontal com-
359 ponents. These terms are similar for both the ESNA and SPNA. The vertical diffusion
360 across 200 m dominates horizontal diffusion. Combined with the advection term, it is
361 the vertical diffusion that drives the salt mass anomaly during 1995–2000 to increase,
362 thereby reversing the fresh anomaly of the 1990s. It also drives the reversal in the salt
363 mass anomaly for 2004–2012. At this time, a decrease in the advection term brings the
364 salt mass anomaly below zero, initiating the F_2 event in both basins (see Fig. 7). The
365 jumps in the vertical diffusion term, which appear as staircases in the time series, are
366 associated with winter-time deep mixing events. The purple mixed layer depth timeseries
367 in Fig. 10 shows this association.

368   **3.4 Variation of Budget Terms With Depth**

369   As the total advection and vertical diffusion terms are of the same magnitude, we
370 investigate their sensitivity to varying the depth of the control volume from its nomi-
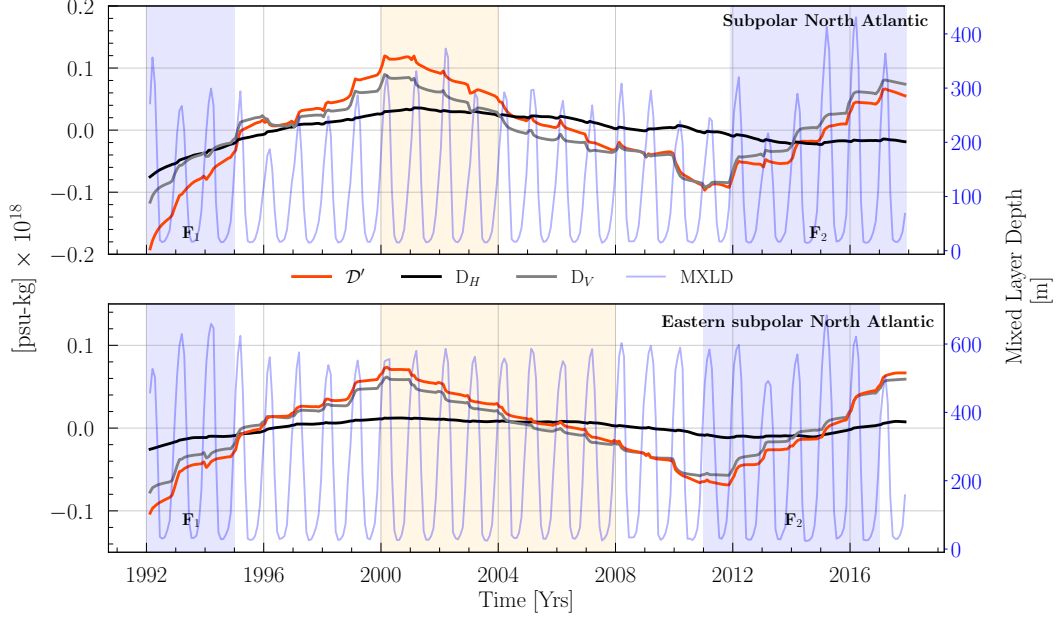371 nal value of 200 m. Fig. 11 shows the change in the ESNA advective and diffusive con-

Figure 10: Decomposition of the diffusion term ($\mathcal{D}'$) in the anomalous salt mass budget for the upper 200 m of the (a) Subpolar North Atlantic and (b) Eastern subpolar North Atlantic (ESNA, see Fig. 2 for the definition of the ESNA). Decomposition terms include horizontal (D_H) and vertical diffusion (D_V), as in (4). The area-averaged mixed layer depth for each basin is shown in purple. F_1 and F_2 are fresh anomaly events in the two basins during 1992–1997 and 2012–2017 respectively. Yellow/blue shading indicates periods of increased/decreased advection of salt mass.

vergence as the integration depth of the bottom of the control volume increases from 10 m to 5500 m. With increasing depth of integration, the contribution of the total diffusive flux in the salt tendency increases and then decreases, reaching a peak at 200 m, which is the nominal value. For integration depths greater than 200 m, there is a trade–off (anti-correlation) between the contribution of the advective convergence term and the diffusive convergence term. For a control volume spanning the whole water column (integration depth of 5500 m), the diffusion term is small and advection dominates. Fig. 11 contextualizes the nominal value of 200 m used to study freshening in the ESNA by Holliday et al. (2020); J. Zhang et al. (2021) and Fox et al. (2022). From a salt budget perspective, the choice of 200 m maximizes the role of diffusion in modulating the salinity anomalies in the ESNA.

3.5 Role of Precipitation, Evaporation, and Runoff

Performing a salt budget analysis for a control volume in the ocean does not account for changes in the salinity due to surface freshwater exchange, i.e., precipitation (P), evaporation (E), and runoff (R). To account for freshwater forcing from the atmosphere, ECCOv4r4 provides a diagnostic representing P-E fluxes and freshwater input from river runoff, R. We use the seawater volume budget and the salt budget to estimate the contribution of P-E+R in changing the salinity in the ESNA and SPNA. The volume conservation in ECCOv4r4 is (Forget et al. (2015); see their equation 3)

$$\frac{1}{H}\frac{\partial \eta}{\partial t} = -\nabla_{z^\star} \cdot s^\star \mathbf{v} - \frac{\partial w}{\partial z^\star} + s^\star \mathcal{F}. \tag{5}$$
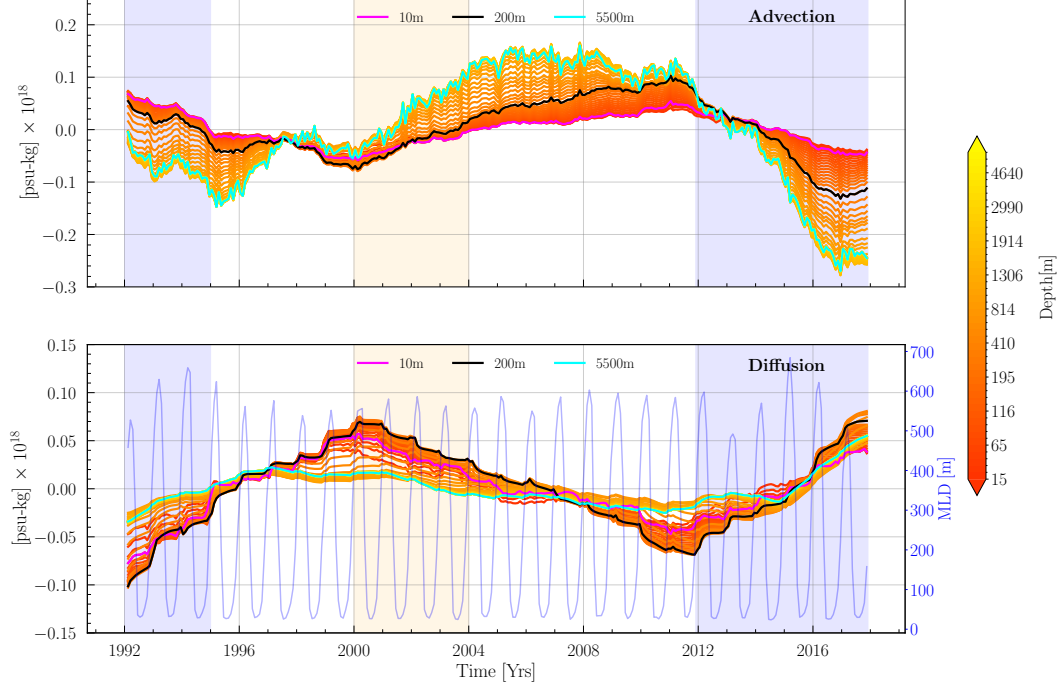
Figure 11: Variation of the advection and diffusion term (horizontal diffusion D_H and vertical diffusion D_V) with depth of the ESNA control volume used in the salt mass budget analysis. The 50 ECCO depth levels (from 10 m to 5000 m) are plotted. The black line denotes the 200 m isobath and the cyan and magenta lines denote 10 m and 5500 m depth levels respectively. F_1 and F_2 are fresh anomaly events in the two basins during 1992–1997 and 2012–2017 respectively. Yellow/blue shading indicates periods of increased/decreased advection of salt mass.

Here, η is the sea surface height, $\mathbf{v} = (u_e, v_e, w_e)$ are the horizontal and vertical Eulerian velocity components. The other terms are the same as those in Eq. (A1). Eq. (5) expresses that the rate of change of the volume is a sum of surface freshwater forcing and advective volume-flux divergence. Integration of Eq. (5) in space and time is used to calculate the volume-integrated anomaly in the total mass of the ESNA and SPNA (ECCOv4r4 makes the Boussinesq approximation, so seawater volume is proportional to seawater mass). As Eq. (1), we express this as

$$M_s(t) \equiv \underbrace{\int^t \int_V \rho_0 \; dV^\star \; dt}_{\text{Seawater Mass}} = \underbrace{\rho_0 \int^t \int_V -\nabla_{z^\star} \cdot (s^\star \mathbf{v}) - \frac{\partial(w)}{\partial z^\star} \; dV^\star \; dt}_{\text{Advection}}$$

$$+ \underbrace{\rho_0 \int^t \int_V s^\star \mathcal{F} \; dV^\star \; dt}_{\text{Forcing}}. \quad (6)$$

Similar to the salt mass anomaly analysis, we remove the seasonality and long term trends from the seawater mass time series $M_s(t)$. This gives us the time integrated seawater mass anomaly, which is shown in Fig. 12 (labelled "seawater anomaly"). We find that the total mass of the SPNA and the ESNA does not change significantly over 1992–2017. This is due to a compensation between the anomalous P-E+R and the convergence of mass over the basins. Josey and Marsh (2005) and Holliday et al. (2020) show that the ESNA received anomalous positive P-E+R, which was primarily precipitation (P) during 1992–

410   1999 and 2012–2017. This is balanced by an increased mass flux exiting the basin dur-
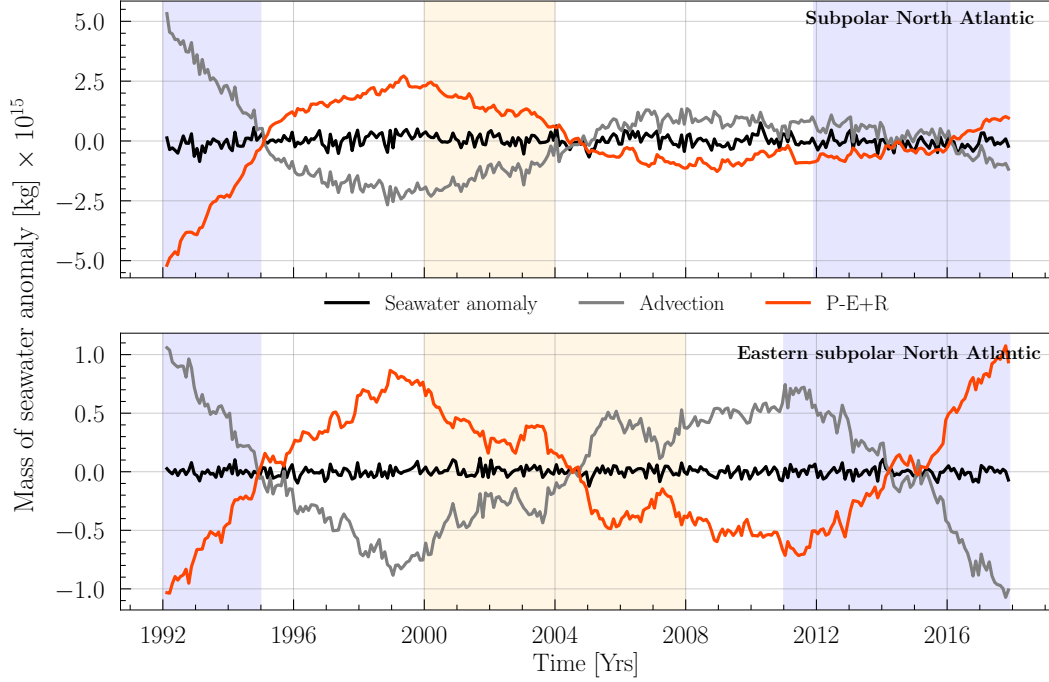411   ing the same period.

Figure 12: (a) Seawater mass anomaly budget for the upper 200 m of the (a) Subpolar North Atlantic and (b) the eastern subpolar North Atlantic (ESNA, see Fig. 2 for the definition of the ESNA). F_1 and F_2 are fresh anomaly events in the two basins during 1992–1997 and 2012–2017 respectively. Yellow/blue shading indicates periods of increased/decreased advection of salt mass.

412   We can now decompose the total contribution to changes in the average salinity
413   of the control volume using a combination of the salt mass and seawater mass budget.
414   We express the salt tendency in the salt conservation equation using

$$\frac{\partial (s^\star S)}{\partial t} = s^\star \frac{\partial S}{\partial t} + S \frac{\partial s^\star}{\partial t} \tag{7}$$

417   and

$$\frac{\partial s^\star}{\partial t} = \frac{1}{H} \frac{\partial \eta}{\partial t} \tag{8}$$

420   (from the definition of $s^\star$). Along with Eq. (5), we can rewrite the salt conservation equa-
421   tion (A1) as an equation for the tendency of salinity (similar to equation (12) in Piecuch
422   (2017)), namely,

$$\frac{\partial S}{\partial t} = \frac{1}{s^\star} \underbrace{\left[S \nabla_{z^\star} \cdot (s^\star \mathbf{v}) + S \frac{\partial w}{\partial z^\star} - \nabla_{z^\star} \cdot (s^\star S \mathbf{v}_{res}) - S \frac{\partial w_{res}}{\partial z^\star} \right] + D_s + \mathcal{F}_s}_{\Delta S_{Ocean}} - \underbrace{SF}_{\Delta S_{Atm.}} . \tag{9}$$

425   We integrate Eq. (9) in space and time, remove the seasonality and long term trends
426   from the salinity time series to get the changes in salinity over the SPNA and the ESNA.
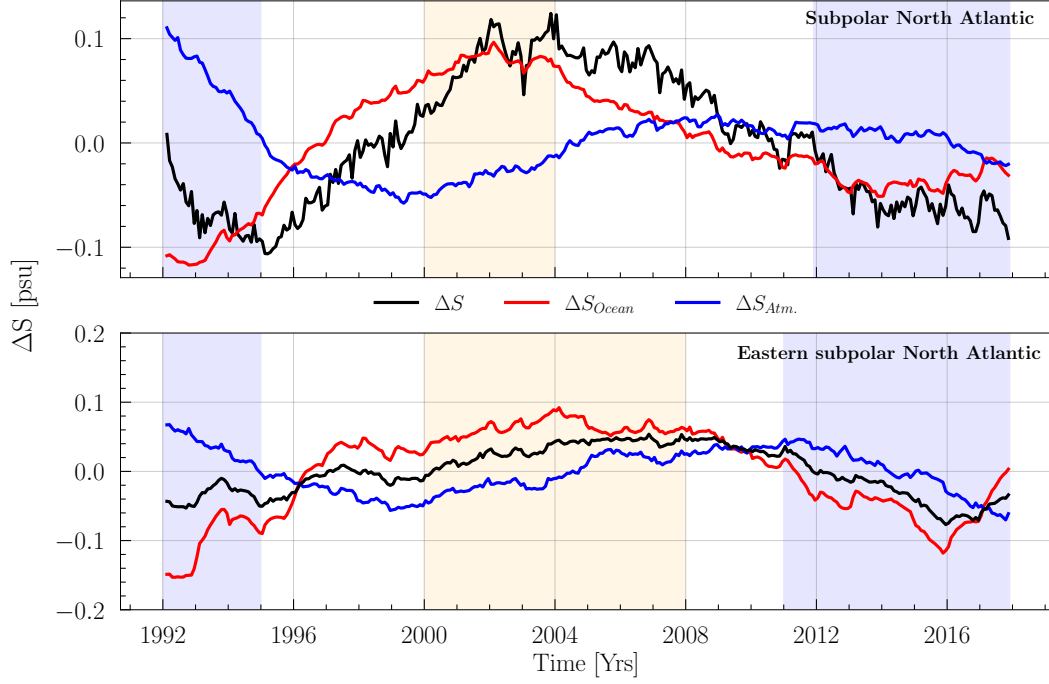427   This is shown in Fig. 13 (labelled "ΔS"). We sum the contributions of ocean advection,

Figure 13: Salinity contribution from the atmosphere and ocean for the upper 200 m of the (a) Subpolar North Atlantic and (b) the eastern subpolar North Atlantic (ESNA, see Fig. 2 for the definition of the ESNA). F_1 and F_2 are fresh anomaly events in the two basins during 1992–1997 and 2012–2017 respectively. Yellow/blue shading indicates periods of increased/decreased advection of salt mass.

diffusion and surface salt exchange and call it ΔS_{Ocean}. The contribution of surface freshwater exchange is labelled $\Delta S_{Atm.}$.

For the SPNA, we find that the precipitation plays an important role during F_1, but not during F_2. After the F_1 event, the changes in salinity are due to ocean advection and diffusion. For the ESNA, precipitation is important for both the fresh anomaly events. Josey and Marsh (2005) and Holliday et al. (2020) conclude the same for the Iceland basin.

4 Discussion

Anomalous low salinity events in the upper 200 m eastern subpolar North Atlantic during the 1990s (F_1) and 2010s (F_2) appear to be qualitatively similar when observed as salinity anomaly signals. Using salt mass budget analysis in the ECCOv4r4 state estimate, we distinguish between the two events and conclude the following:

1. The fresh anomaly in the 1990s (F_1) occurs due to anomalous circulation of mean salinity ($v'\bar{S}$). This primarily occurs as the Eulerian component of $v'\bar{S}$ across the southern and western boundaries and the bolus component of the vertical flux of $v'\bar{S}$ across the 200 m horizon in the ESNA (Fig. 9).
2. The fresh anomaly during 2012–2017 (F_2) is due to the mean circulation of anomalous salinity ($\bar{v}S'$). This is entirely due to the Eulerian component of $\bar{v}S'$ across the western face of the Iceland Basin (Fig. 9).

3. Vertical diffusive flux across the 200 m depth boundary reverses the freshening after F_1 by increasing the salt mass content during 1995–2000. It also controls the salinity during the period leading up to the F_2 event (Fig. 10).

Therefore, although the two salinity anomalies are similar, they do not share the same mechanisms. The Great Salinity Anomaly (GSA) event (F_1) as described in Belkin (2004) propagates via the Labrador Sea and into the Iceland Basin in the mid 1990s. The fresh anomaly observed in the ESNA in the mid 2010s (F_2) has similar characteristics. The difference between the two is that F_2 is dominated by circulation of anomalous salinity along mean currents into the Iceland Basin and F_1 is dominated by anomalous circulation of mean salinity (Fig. 8).

We note that vertical diffusion has an important role to play in driving the negative salinity anomalies to positive salinity anomalies. The 200 m isobath becomes significant in pushing salt flux into the upper layer of the ocean. As we increase the vertical depth of integration in the salt budget, the vertical exchange of salt via diffusion decreases and the horizontal advective exchange increases. Sanders et al. (2022) conduct a similar study to investigate the 2015 anomalous cooling in the eastern and central SPNA (defined over 50–20°W, 43–63°N, which overlaps with, but extends further west than, our definition of the ESNA, Fig. 2). They analyze the heat budget averaged over the mixed layer using ECCOv4r3 and ECCOv4r4. They observe surface heat loss to initiate and drive the cooling, with advection sustaining the anomaly in the region (as expected from Tesdal and Abernathey (2021)). They also emphasize the role of vertical diffusion across the base of the mixed layer in the re-emergence of the anomaly during summer of 2014. The importance of horizontal advection and vertical diffusion for the temperature anomalies is similar to the importance of these processes for the salinity anomalies studied here (Fig 9).

The surface freshwater fluxes (P-E+R) play a significant role in enhancing the fresh anomalies in the ESNA during the F_2 event. This was also noted by Holliday et al. (2020).

Holliday et al. (2020) state that the 2010s (F_2) event does not share the same characteristics of the 20th century GSAs. They argue that this event shows no freshening in the Labrador Sea, unlike GSAs (Belkin (2004); Sundby and Drinkwater (2007)). However, in the ECCOv4r3 freshwater budget for the Labrador Sea explored by Tesdal and Haine (2020) there is an increased freshwater flux from the Labrador Sea via the Labrador Current. This compensates an increased freshwater flux across the Davis Strait so that little net salinity change occurs in the Labrador Sea over this period. Still, recent papers argue that the 2010s (F_2) freshening event resembles a GSA. Specifically, Devana et al. (2021) observe that salinity decrease from November 2015 to March 2017 in the Iceland-Scotland Overflow Water is similar to the freshening observed in the 1990s. Also, Biló et al. (2022) note that the salinity decrease during 2016–2019 in the Irminger Sea (0.04 psu year^{-1}), following the freshening in the Iceland basin, is among the highest ever recorded.

Realistic, physically-consistent state estimates, such as ECCOv4r4 and ASTE_1 used here, are valuable to diagnose mechanisms of large-scale inter-annual salinity and temperature fluctuations because closed volume, heat, and salt budgets can be constructed. Apart from possible bias (section 3.1), such state estimates have some drawbacks, however. State estimates do not include error estimates in the model output fields, for instance (Piecuch et al., 2017). Tesdal and Haine (2020) address this issue by using $\pm$ 2 standard deviations of the monthly lateral ECCO fluxes as a substitute for formal uncertainty estimates. Another limitation is that state estimates typically span a relatively short period (1992–2017 in the case of ECCOv4r4). Therefore, investigations of low-frequency (decadal to centennial) salinity and temperature variability are not possible with these products.

For future studies, it is important to investigate such low-frequency fluctuations in the ESNA. Notably, the importance of the meridional overturning circulation, which has not been addressed in this study, and atmospheric forcing needs further attention. Coupled climate models are a promising resource for these studies because they also allow construction of closed volume, heat, and salt budgets, but with much longer durations.

5 Data Availability Statement

We use an open source python package, OceanSpy (`https://oceanspy.readthedocs.io`; Almansi et al., 2019), to create and analyze synthetic hydrographic sections in the model data. We also use the python package gcm-filters (`https://gcm-filters.readthedocs.io`; Loose et al., 2022) to apply spatial Gaussian filters for smoothing the AVISO data. The ECCO dataset is publicly available on the SciServer system (Medvedev et al., 2016) and at `https://podaac.jpl.nasa.gov/ECCO`. ASTE_1 data is publicly available on `https://arcticdata.io/catalog/portals/ASTE`. The EN4 data are available at `www.metoffice.gov.uk/hadobs/en4/`. Python scripts with Juptyer notebooks used for analyzing ECCO budgets can be accessed at `https://github.com/asiddi24/Siddiqui_et_al_JGR_Oceans_2024` along with scripts used for generating all figures in the manuscript.

Appendix A Salt Budget equations

This appendix is useful in understanding the formulation of Eqs. (1, 2, 3). The $z^\star$ coordinate is used in ECCOv4r4 to allow for exact tracer conservation (Campin et al., 2004) and to improve representation of flow over steep topography (Adcroft & Campin, 2004). Physically, $z^\star$ allows for variations in the non-linear free surface to be distributed throughout the vertical water column. Using this coordinate, Forget et al. (2015) express the salt conservation equation as

$$\frac{\partial(s^\star S)}{\partial t} = -\nabla_{z^\star} \cdot (s^\star S \mathbf{v}_{res}) - \frac{\partial(S\, w_{res})}{\partial z^\star} + s^\star (\mathcal{F}_S + D_{\sigma,S} + D_{\perp,S}). \tag{A1}$$

Integrating Eq. (A1) over a spatial domain V and over time yields a time series for the salt mass, $M(t)$, expressed in Eq. (1).

For the anomalous advection term, $\mathcal{A}'$, consider

$$\mathbf{v}_{res} = \bar{\mathbf{v}}_{res} + \mathbf{v}'_{res},$$
$$w_{res} = \bar{w}_{res} + w'_{res},$$
$$S = \bar{S} + S',$$

This decomposition implies that

$$\bar{\mathbf{v}}_{res}\bar{S} = \overline{\mathbf{v}_{res}S} - \overline{\mathbf{v}'_{res}S'},$$
$$\bar{w}_{res}\bar{S} = \overline{w_{res}S} - \overline{w'_{res}S'}.$$

The anomalous advection term is therefore:

$$\mathcal{A}' = -\rho_0 \int^t \int_V \nabla_{z^\star} \cdot \left[\left(s^\star (\bar{\mathbf{v}}_{res}S' + \mathbf{v}'_{res}\bar{S} + \mathbf{v}'_{res}S' - \overline{\mathbf{v}'_{res}S'}) \right] \, dV^\star \, dt^\star \right.$$
$$- \rho_0 \int^t \int_V \frac{\partial(\bar{w}_{res}S' + w'_{res}\bar{S} + w'_{res}S' - \overline{w'_{res}S'})}{\partial z^\star} \, dV^\star \, dt^\star. \tag{A2}$$

This is rearranged in Eq. (2).

References

Adcroft, A., & Campin, J.-M. (2004). Rescaled height coordinates for accurate representation of free-surface flows in ocean circulation models. *Ocean Modelling*, *7*(3), 269-284. doi: https://doi.org/10.1016/j.ocemod.2003.09.003

Almansi, M., Gelderloos, R., Haine, T. W. N., Saberi, A., & Siddiqui, A. H. (2019). Oceanspy: A Python package to facilitate ocean model data analysis and visualization. *Journal of Open Source Software*, *4*(39), 1506. doi: https://doi.org/10.21105/joss.01506

Belkin, I. M. (2004). Propagation of the Great Salinity Anomaly of the 1990s around the northern North Atlantic. *Geophysical Research Letters*, *31*(8). doi: https://doi.org/10.1029/2003GL019334

Belkin, I. M., Levitus, S., Antonov, J., & Malmberg, S.-A. (1998). Great Salinity Anomalies in the North Atlantic. *Progress in Oceanography*, *41*(1), 1 - 68. doi: https://doi.org/10.1016/S0079-6611(98)00015-9

Biló, T. C., Straneo, F., Holte, J., & Le Bras, I. A.-A. (2022). Arrival of New Great Salinity Anomaly Weakens Convection in the Irminger Sea. *Geophysical Research Letters*, *49*(11), e2022GL098857. (e2022GL098857 2022GL098857) doi: https://doi.org/10.1029/2022GL098857

Bryden, H. L., Johns, W. E., King, B. A., McCarthy, G., McDonagh, E. L., Moat, B. I., & Smeed, D. A. (2020). Reduction in Ocean Heat Transport at 26°N since 2008 Cools the Eastern Subpolar Gyre of the North Atlantic Ocean. *Journal of Climate*, *33*(5), 1677 - 1689. doi: https://doi.org/10.1175/JCLI-D-19-0323.1

Buckley, M. W., Ponte, R. M., Forget, G., & Heimbach, P. (2014). Low-Frequency SST and Upper-Ocean Heat Content Variability in the North Atlantic. *Journal of Climate*, *27*(13), 4996 - 5018. doi: https://doi.org/10.1175/JCLI-D-13-00316.1

Buckley, M. W., Ponte, R. M., Forget, G., & Heimbach, P. (2015). Determining the Origins of Advective Heat Transport Convergence Variability in the North Atlantic. *Journal of Climate*, *28*(10), 3943 - 3956. doi: https://doi.org/10.1175/JCLI-D-14-00579.1

Burkholder, K. C., & Lozier, M. S. (2014). Tracing the pathways of the upper limb of the North Atlantic Meridional Overturning Circulation. *Geophysical Research Letters*, *41*(12), 4254-4260. doi: https://doi.org/10.1002/2014GL060226

Campin, J.-M., Adcroft, A., Hill, C., & Marshall, J. (2004). Conservation of properties in a free-surface model. *Ocean Modelling*, *6*(3), 221-244. doi: https://doi.org/10.1016/S1463-5003(03)00009-X

Chafik, L., Nilsen, J. E. Ø., Dangendorf, S., Reverdin, G., & Frederikse, T. (2019). North atlantic ocean circulation and decadal sea level change during the altimetry era. *Scientific reports*, *9*(1), 1–9. doi: https://doi.org/10.1038/s41598-018-37603-6

Daniault, N., Mercier, H., Lherminier, P., Sarafanov, A., Falina, A., Zunino, P., . . . Gladyshev, S. (2016). The northern North Atlantic Ocean mean circulation in the early 21st century. *Progress in Oceanography*, *146*, 142-158. doi: https://doi.org/10.1016/j.pocean.2016.06.007

Devana, M. S., Johns, W. E., Houk, A., & Zou, S. (2021). Rapid freshening of ice-

land scotland overflow water driven by entrainment of a major upper ocean salinity anomaly. *Geophysical Research Letters*, *48*(22), e2021GL094396. (e2021GL094396 2021GL094396) doi: https://doi.org/10.1029/2021GL094396

Dickson, R. R., Meincke, J., Malmberg, S.-A., & Lee, A. J. (1988). The great salinity anomaly in the Northern North Atlantic 1968-1982. *Progress in Oceanography*, *20*(2), 103 - 151. doi: https://doi.org/10.1016/0079-6611(88)90049-3

Doney, S. C., Yeager, S., Danabasoglu, G., Large, W. G., & McWilliams, J. C. (2007). Mechanisms Governing Interannual Variability of Upper-Ocean Temperature in a Global Ocean Hindcast Simulation. *Journal of Physical Oceanography*, *37*(7), 1918 - 1938. doi: https://doi.org/10.1175/JPO3089.1

Dong, B., & Sutton, R. (2002). Variability in North Atlantic heat content and heat transport in a coupled ocean–atmosphere GCM. *Climate Dynamics*, *19*(5–6), 485–497. doi: https://doi.org/10.1007/s00382-002-0239-7

Dooley, H., Martin, J., & Ellett, D. (1984). Abnormal hydrographic conditions in the Northeast Atlantic during the 1970s. *Rapp PV Reun Cons Int Explor Mer*, *185*, 179–187.

ECCO Consortium, I., Fukumori, Wang, O., Fenty, I., Forget, P., G.and Heimbach, & Ponte, R. M. (n.d.). ECCO Central Estimate (Version 4 Release 4). Retrieved from https://ecco.jpl.nasa.gov/drive/files/version4/release4.

Forget, G., Campin, J.-M., Heimbach, P., Hill, C. N., Ponte, R. M., & Wunsch, C. (2015). ECCO version 4: an integrated framework for non-linear inverse modeling and global ocean state estimation. *Geoscientific Model Development*, *8*(10), 3071–3104. doi: https://doi.org/10.5194/gmd-8-3071-2015

Foukal, N. P., & Lozier, M. S. (2017). Assessing variability in the size and strength of the North Atlantic subpolar gyre. *Journal of Geophysical Research: Oceans*, *122*(8), 6295-6308. doi: https://doi.org/10.1002/2017JC012798

Foukal, N. P., & Lozier, M. S. (2018). Examining the Origins of Ocean Heat Content Variability in the Eastern North Atlantic Subpolar Gyre. *Geophysical Research Letters*, *45*(20), 11,275-11,283. doi: https://doi.org/10.1029/2018GL079122

Fox, A. D., Handmann, P., Schmidt, C., Fraser, N., Rühs, S., Sanchez-Franks, A., . . . Yashayaev, I. (2022). Exceptional freshening and cooling in the eastern subpolar North Atlantic caused by reduced Labrador Sea surface heat loss. *Ocean Science*, *18*(5), 1507–1533. doi: https://doi.org/10.5194/os-18-1507-2022

Good, S. A., Martin, M. J., & Rayner, N. A. (2013). EN4: Quality controlled ocean temperature and salinity profiles and monthly objective analyses with uncertainty estimates. *Journal of Geophysical Research: Oceans*, *118*(12), 6704-6716. doi: https://doi.org/10.1002/2013JC009067

Holliday, N. P. (2003). Air-sea interaction and circulation changes in the northeast Atlantic. *Journal of Geophysical Research: Oceans*, *108*(C8). doi: https://doi.org/10.1029/2002JC001344

Holliday, N. P., Bersch, M., Berx, B., Chafik, L., Cunningham, S., Cristian, F.-L., . . . Yashayaev, I. (2020). Ocean circulation causes the largest freshening event for 120 years in eastern subpolar North Atlantic. *Nature Communications*, *11*. doi: https://doi.org/10.1038/s41467-020-14474-y

Holliday, N. P., & Cunningham, S. A. (2013). The Extended Ellett Line: Discoveries from 65 Years of Marine Observations West of the UK. *Oceanography*, *26*(2), 156–163.

Hátún, H., Payne, M., Beaugrand, G., Reid, P., Sandø, A., Drange, H., . . . Bloch, D. (2009). Large bio-geographical shifts in the north-eastern Atlantic Ocean: From the subpolar gyre, via plankton, to blue whiting and pilot whales. *Progress in Oceanography*, *80*(3), 149-162. doi: https://doi.org/10.1016/j.pocean.2009.03.001

Hátún, H., Sandø, A. B., Drange, H., Hansen, B., & Valdimarsson, H. (2005). Influence of the Atlantic Subpolar Gyre on the Thermohaline circulation. *Science*, *309*(5742), 1841-1844. doi: https://doi.org/10.1126/science.1114777

Häkkinen, S., & Rhines, P. B. (2004). Decline of Subpolar North Atlantic Circulation During the 1990s. *Science*, *304*(5670), 555-559. doi: https://doi.org/10.1126/science.1094917

Häkkinen, S., Rhines, P. B., & Worthen, D. L. (2011). Warm and saline events embedded in the meridional circulation of the northern North Atlantic. *Journal of Geophysical Research: Oceans*, *116*(C3). doi: https://doi.org/10.1029/2010JC006275

Josey, S. A., & Marsh, R. (2005). Surface freshwater flux variability and recent freshening of the North Atlantic in the eastern subpolar gyre. *Journal of Geophysical Research: Oceans*, *110*(C5). doi: https://doi.org/10.1029/2004JC002521

Joyce, T. M., & Zhang, R. (2010). On the Path of the Gulf Stream and the Atlantic Meridional Overturning Circulation. *Journal of Climate*, *23*(11), 3146 - 3154. doi: https://doi.org/10.1175/2010JCLI3310.1

Koul, V., Tesdal, J.-E., Bersch, M., Hátún, H., Brune, S., Borchert, L., ... Baehr, J. (2020). Unraveling the choice of the north Atlantic subpolar gyre index. *Scientific reports*, *10*(1), 1–12. doi: https://doi.org/10.1038/s41598-020-57790-5

Loose, N., Abernathey, R., Grooms, I., Busecke, J., Guillaumin, A., Yankovsky, E., ... Martin, P. (2022). GCM-Filters: A Python Package for Diffusion-based Spatial Filtering of Gridded Data. *Journal of Open Source Software*, *7*(70), 3947. doi: https://doi.org/10.21105/joss.03947

Medvedev, D., Lemson, G., & Rippin, M. (2016). Sciserver Compute: Bringing Analysis Close to the Data. In *Proceedings of the 28th international conference on scientific and statistical database management.* New York, NY, USA: Association for Computing Machinery. doi: https://doi.org/10.1145/2949689.2949700

Nguyen, A. T., Pillar, H., Ocaña, V., Bigdeli, A., Smith, T. A., & Heimbach, P. (2021). The Arctic Subpolar Gyre sTate Estimate: Description and Assessment of a Data-Constrained, Dynamically Consistent Ocean-Sea Ice Estimate for 2002–2017. *Journal of Advances in Modeling Earth Systems*, *13*(5), e2020MS002398. (e2020MS002398 2020MS002398) doi: https://doi.org/10.1029/2020MS002398

Nye, J. A., Joyce, T. M., Kwon, Y.-O., & Link, J. S. (2011). Silver hake tracks changes in Northwest Atlantic circulation. *Nature communications*, *2*(1), 412. doi: https://doi.org/10.1038/ncomms1420

Oldenburg, D., Armour, K. C., Thompson, L., & Bitz, C. M. (2018). Distinct Mechanisms of Ocean Heat Transport Into the Arctic Under Internal Variability and Climate Change. *Geophysical Research Letters*, *45*(15), 7692-7700. doi: https://doi.org/10.1029/2018GL078719

Piecuch, C. G. (2017). *A note on practical evaluation of budgets in ECCO version 4 release 3* (Tech. Rep.). Retrieved from `http://hdl.handle.net/1721.1/111094`

Piecuch, C. G., Ponte, R. M., Little, C. M., Buckley, M. W., & Fukumori, I. (2017). Mechanisms underlying recent decadal changes in subpolar North Atlantic Ocean heat content. *Journal of Geophysical Research: Oceans*, *122*(9), 7181-7197. doi: https://doi.org/10.1002/2017JC012845

Reverdin, G., Niiler, P. P., & Valdimarsson, H. (2003). North Atlantic Ocean surface currents. *Journal of Geophysical Research: Oceans*, *108*(C1), 2-1-2-21. doi: https://doi.org/10.1029/2001JC001020

Sanchez-Franks, A., & Zhang, R. (2015). Impact of the Atlantic meridional overturning circulation on the decadal variability of the Gulf Stream path and regional chlorophyll and nutrient concentrations. *Geophysical Research Letters*, *42*(22), 9889-9887. doi: https://doi.org/10.1002/2015GL066262

Sanders, R. N. C., Jones, D. C., Josey, S. A., Sinha, B., & Forget, G. (2022). Causes of the 2015 North Atlantic cold anomaly in a global state estimate. *Ocean Sci-*

ence, *18*(4), 953–978. doi: https://doi.org/10.5194/os-18-953-2022

Sarafanov, A., Falina, A., Sokov, A., & Demidov, A. (2008). Intense warming and salinification of intermediate waters of southern origin in the eastern subpolar North Atlantic in the 1990s to mid-2000s. *Journal of Geophysical Research: Oceans*, *113*(C12). doi: https://doi.org/10.1029/2008JC004975

Schauer, U., & Losch, M. (2019). "Freshwater" in the Ocean is Not a Useful Parameter in Climate Research. *Journal of Physical Oceanography*, *49*(9), 2309 - 2321. doi: https://doi.org/10.1175/JPO-D-19-0102.1

Sundby, S., & Drinkwater, K. (2007). On the mechanisms behind salinity anomaly signals of the northern North Atlantic. *Progress in Oceanography*, *73*(2), 190 - 202. doi: https://doi.org/10.1016/j.pocean.2007.02.002

Tesdal, J.-E., & Abernathey, R. P. (2021). Drivers of Local Ocean Heat Content Variability in ECCOv4. *Journal of Climate*, *34*(8), 2941 - 2956. doi: https://doi.org/10.1175/JCLI-D-20-0058.1

Tesdal, J.-E., Abernathey, R. P., Goes, J. I., Gordon, A. L., & Haine, T. W. N. (2018). Salinity Trends within the Upper Layers of the Subpolar North Atlantic. *Journal of Climate*, *31*(7), 2675 - 2698. doi: https://doi.org/10.1175/JCLI-D-17-0532.1

Tesdal, J.-E., & Haine, T. W. N. (2020). Dominant Terms in the Freshwater and Heat Budgets of the Subpolar North Atlantic Ocean and Nordic Seas From 1992 to 2015. *Journal of Geophysical Research: Oceans*, *125*(10), e2020JC016435. doi: https://doi.org/10.1029/2020JC016435

Thierry, V., de Boisséson, E., & Mercier, H. (2008). Interannual variability of the Subpolar Mode Water properties over the Reykjanes Ridge during 1990–2006. *Journal of Geophysical Research: Oceans*, *113*(C4). doi: https://doi.org/10.1029/2007JC004443

Weijer, W., Haine, T. W., Siddiqui, A. H., Cheng, W., Veneziani, M., & Kurtakoti, P. (2022, December). Interactions between the arctic mediterranean and the atlantic meridional overturning circulation: A review. *Oceanography*.

Yan, X., Zhang, R., & Knutson, T. R. (2017). The role of Atlantic overturning circulation in the recent decline of Atlantic major hurricane frequency. *Nature Communications*, *8*(1), 1695. doi: https://doi.org/10.1038/s41467-017-01377-8

Yan, X., Zhang, R., & Knutson, T. R. (2018). Underestimated AMOC Variability and Implications for AMV and Predictability in CMIP Models. *Geophysical Research Letters*, *45*(9), 4319-4328. doi: https://doi.org/10.1029/2018GL077378

Yeager, S. (2015). Topographic Coupling of the Atlantic Overturning and Gyre Circulations. *Journal of Physical Oceanography*, *45*(5), 1258 - 1284. doi: https://doi.org/10.1175/JPO-D-14-0100.1

Yeager, S., Karspeck, A., Danabasoglu, G., Tribbia, J., & Teng, H. (2012). A Decadal Prediction Case Study: Late Twentieth-Century North Atlantic Ocean Heat Content. *Journal of Climate*, *25*(15), 5173 - 5189. doi: https://doi.org/10.1175/JCLI-D-11-00595.1

Zhang, J., Weijer, W., Steele, M., Cheng, W., Verma, T., & Veneziani, M. (2021). Labrador Sea freshening linked to Beaufort Gyre freshwater release. *Nature communications*, *12*(1), 1–8. doi: https://doi.org/10.1038/s41467-021-21470-3

Zhang, R. (2008). Coherent surface-subsurface fingerprint of the Atlantic meridional overturning circulation. *Geophysical Research Letters*, *35*(20). doi: https://doi.org/10.1029/2008GL035463

Zhang, R., & Vallis, G. K. (2006). Impact of Great Salinity Anomalies on the Low-Frequency Variability of the North Atlantic Climate. *Journal of Climate*, *19*(3), 470 - 482. doi: https://doi.org/10.5194/gmd-8-3071-201510.1175/JCLI3623.1